fuels

MDPI

Article

Numerical Analysis on Impact of Membrane Thickness and Temperature on Characteristics of Biogas Dry Reforming Membrane Reactor Using Pd/Cu Membrane and Ni/Cr Catalyst

Akira Nishimura [1,*], Ryoma Ichii [1], Souta Yamada [1], Mizuki Ichikawa [1], Taisei Hayakawa [1] and Eric Hu [2]

[1] Division of Mechanical Engineering, Mie University, Tsu 514-8507, Japan; 424m107@m.mie-u.ac.jp (R.I.); 423m161@m.mie-u.ac.jp (S.Y.); 424m108@m.mie-u.ac.jp (M.I.); 421027@m.mie-u.ac.jp (T.H.)

[2] School of Electrical and Mechanical Engineering, the University of Adelaide, Adelaide, SA 5005, Australia; eric.hu@adelaide.edu.au

* Correspondence: nisimura@mach.mie-u.ac.jp; Tel.:+81-59-231-9747

Abstract: The purpose of this study is to reveal the characteristics of a Pd/Cu membrane and Ni/Cr catalyst adopted in a biogas dry reforming (BDR) membrane reactor by the numerical simulation procedure. The commercial software COMSOL Multiphysics ver. 6.2 was adopted in the numerical simulation. COMSOL is one type of commercial software that can solve multiphysics phenomena, i.e., chemical reaction, fluid dynamics, heat transfer, etc. The impact of the initial reaction temperature and the thickness of the Pd/Cu membrane on the performance of the BDR membrane reactor using an Ni/Cr catalyst is also investigated. The initial reaction temperatures adopted were 400 °C, 500 °C, and 600 °C, and the thicknesses of the Pd/Cu membrane were varied at 20 μm, 40 μm, and 60 μm. It was discovered that when the initial reaction temperature was raised, the molar concentration of H_2 increased while the molar concentrations of CH_4 and CO_2 decreased. Because the penetration resistance of the Pd/Cu membrane decreased with the decrease in the thickness of the Pd/Cu membrane, the molar concentrations of H_2 remaining in the Pd/Cu membrane and sweep chamber rose with the decrease in the thickness of the Pd/Cu membrane.

Keywords: biogas dry reforming; membrane reactor type; numerical simulation; thickness of membrane; Ni/Cr catalyst

check for updates

Academic Editor: Yoonah Jeong

Received: 2 January 2025
Revised: 27 January 2025
Accepted: 31 March 2025
Published: 3 April 2025

Citation: Nishimura, A.; Ichii, R.; Yamada, S.; Ichikawa, M.; Hayakawa, T.; Hu, E. Numerical Analysis on Impact of Membrane Thickness and Temperature on Characteristics of Biogas Dry Reforming Membrane Reactor Using Pd/Cu Membrane and Ni/Cr Catalyst. *Fuels* **2025**, *6*, 25. https://doi.org/10.3390/fuels6020025

Copyright: © 2025 by the authors. Licensee MDPI, Basel, Switzerland. This article is an open access article distributed under the terms and conditions of the Creative Commons Attribution (CC BY) license (https://creativecommons.org/licenses/by/4.0/).

1. Introduction

Green H_2 is one promising procedure to generate a clean energy source in order to solve the global warming issue. There are many technologies to produce green H_2, e.g., H_2O electrolysis and the biogas dry reforming (BDR) membrane reactor using various catalysts. The $Pt_1/(Co, Ni)(OH)_2$ single-atom catalyst with single Pt atoms exhibited very superior H_2 evolution reaction activity to $Pt_1/Co(OH)_2/C$, $Pt_1/Ni(OH)_2/C$, Pt_1/C, and the commercial 20 wt.% Pt/C during H_2O dissociation [1]. In addition, $Pd_{12}Ru_3/Ni(OH)_2/C$ exhibited remarkably decreased H_2 evolution reactions (16.1 mV @ 10 mA/cm^2) as compared with the commercial 20 wt.% Pt/C (26.0 mV @ 10 mA/cm^2) during alkaline H_2O electrolysis [2]. Moreover, Pt/rGNP exhibited better catalytic behavior (10.6 mV @ 100 mA/cm^2) for the H_2 evolution reaction compared to the as-prepared M/rGNP catalyst, which was smaller compared to that of the commercial 20 wt.% Pt/C (66.5 mV) [3]. However, the present study pays attention to biogas dry reforming (BDR) as technology to produce green H_2. Biogas is a type of fuel that consists of CH_4 (55–75 vol.%) and CO_2 (25–45 vol.%) [4], which

can be used as feedback for the BDR reactor. Biogas can be produced from fermentation after the action of anaerobic microorganisms on raw materials such as garbage, livestock excretion, and sewage sludge. In total, 1.46 EJ of biogas was produced in the world in 2020, which was five times as large as the amount of gas produced in 2000 [5]. Consequently, it might be expected that the amount of produced biogas will increase more in the future.

Biogas can be provided as one type of fuel supplied for gas engines and micro gas turbines [6]. However, the power output is naturally lower compared with using natural gas as fuel since its heating value is lower due to including CO_2. This study has suggested a combination system that consists of a BDR reactor combined with a solid oxide fuel cell (SOFC) to solve this problem [7]. CO, which is a by-product from BDR, could be used as fuel for the SOFC. The total energy conversion efficiency is therefore larger than some of the actual power generation systems, such as gas engines and micro gas turbines, since the SOFC can be a co-generation system.

There have been many reported studies on BDR recently [8–15]. The R&D of catalysts is one method to improve the performance of BDR. From a literature survey, this study can claim that Ni-based catalysts were examined for BDR [8–15]. Ni/Ce/Al was developed and performed a CH_4 conversion of 65–79% and a CO_2 conversion of 77–86% at 750 °C [8]. La/Ni/SBA-16 exhibited a CH_4 conversion of 86% and the CO_2 conversion of 92% at 700 °C [9]. The CH_4 conversion and the CO_2 conversion increased with the rise in the reaction temperature from 600 °C to 700 °C. $Ni/CeO_2/Al_2O_3$ performed a CH_4 conversion of approximately 100% and a CO_2 conversion of approximately 100% at 800 °C [10]. Ni/γ-Al_2O_3 exhibited a CH_4 conversion of 90% and a CO_2 conversion of 50% at 800 °C [11]. $Ni/CeZrO_2$ performed a CH_4 conversion of approximately 40% as well as a CO_2 conversion of approximately 55% at 800 °C [12]. The CH_4 conversion and the CO_2 conversion increased with the rise in the reaction temperature from 500 °C to 800 °C. Ni/Al_2O_3 exhibited a CH_4 conversion of approximately 70% and a CO_2 conversion of approximately 70% at 700 °C [13]. Ni/La/Ti performed a CH_4 conversion of approximately 100% and a CO_2 conversion of approximately 100% at 800 °C [14]. The CH_4 conversion and the CO_2 conversion increased from 600 °C to 800 °C, from approximately 78% to 100% and from approximately 55% to 100%, respectively. The thermogravimetric analysis for $Ni/Cao/Al_2O_3$ was investigated, which clarified the effect of heating rate on the H_2 production rate considering some chemical reaction schemes [15]. In the case of increasing the heating rate from 5 K/min to 20 K/min, the maximum H_2 production rate rose from 7×10^{-5} mol/s to 1×10^{-4} mol/s.

Though some Ni-based catalysts were examined, the Ni/Cr catalyst has not been examined sufficiently, excluding some previous studies [7,16].

Moreover, it can be said that it is important to operate at a lower temperature in order to enhance the thermal energy efficiency of BDR, because BDR is an endothermic reaction. It can be thought that a membrane reactor is an effective device to facilitate this purpose since the H_2 production rate of BDR is improved by supplying the non-equilibrium state due to H_2 separation from the reaction site of the catalyst [7]. Pd is known as a material of the H_2 separation membrane [17]. The permeation of H_2 from a high-partial-pressure region to a low-partial-pressure region occurs via the following steps: (a) the dissociative adsorption of H_2 on the interface between the gas and metal; (b) sorption of the atomic H_2 into the bulk metal; (c) diffusion of atomic H_2 by means of the bulk metal membrane; (d) recombination of atomic H_2 to form H_2 molecules at the interface between the gas and metal permeate; (e) desorption of molecular H_2 [17]. Since the cost of pure H_2 is expensive, some Pd alloys are considered a materials of H_2 separation membranes. Though several Pd alloy membranes, e.g., Pd/Ag and Pd/Au, are commercialized and used for research, the cost of Pd/Cu is relatively lower than the cost of Pd/Ag, Pd/Au, and pure Pd. We think that cost is an important factor for applying the proposed system to the industry in

the near future. Therefore, this study selects Pd/Cu as the H_2 separation membrane. It is reported that Pd/Cu was used for the H_2 separation membrane in the previous study [18]. Commercial catalysts such as Al_2O_3, Cr_2O_3, CrO_3, and CuO were used for a water gas shift reaction (WGS) in the previous study. The increase in the conversion rate increased with the steam/carbon ratio from 1 to 3 and became smooth from 4 to 5. The membrane reactor with a Pd/Cu membrane and Ni/Cu catalyst was experimentally investigated by the previous study carried out by the authors of this study [8]. Though a numerical study on BDR with an Ni/Cr catalyst in a rectangular reactor was carried out by the authors of this study [16], this study did not conduct a numerical study to clarify the characteristics of BDR in the membrane reactor with a Pd/Cu membrane and Ni/Cu catalyst.

Therefore, the aim of this study is to reveal the characteristics of BDR in a membrane reactor with a Pd/Cu membrane and Ni/Cr catalyst by numerical simulation. The present study conducts a numerical simulation using the commercial software COMSOL Multiphysics ver. 6.2. Because there are many previous studies conducted by COMSOL Multiphysics for the purpose of the numerical simulation of BDR [19–22], this study has adopted COMSOL Multiphysics for the numerical simulation in this study. The impact of the initial reaction temperature and the thickness of the Pd/Cu membrane on the performance of BDR in the membrane reactor using a Pd/Cu membrane and Ni/Cr catalyst is also investigated. The initial reaction temperature is varied at 400 °C, 500 °C, and 600 °C. The thickness of the Pd/Cu membrane is varied at 20 μm, 40 μm, and 60 μm. A 2D model that simulates the membrane reactor used in the authors' previous studies [7] is adopted in order to shorten the calculation time, though the actual experimental reactor is 3D. The molar ratio of CH_4:CO_2 is set to 1.5:1, simulating a biogas in the present study. To investigate the initial reaction temperature and the thickness of the Pd/Cu membrane on the reaction characteristics of BDR, as well as the other reactions, the following chemical reactions can be considered [8,10,12]:

<Dry reforming reaction (DR)>

$$CH_4 + CO_2 \rightarrow 2H_2 + 2CO + 247\ kJ/mol \quad (1)$$

<Steam reforming reaction (SR)>

$$CH_4 + H_2O \rightarrow CO + 3H_2 + 206\ kJ/mol \quad (2)$$

<Reverse water gas shift reaction (RWGS)>

$$CO_2 + H_2 \rightarrow CO + H_2O + 41\ kJ/mol \quad (3)$$

<Methanation reaction (MR)>

$$CO_2 + 4H_2 \rightarrow CH_4 + 2H_2O - 165.0\ kJ/mol \quad (4)$$

<Methane decomposition reaction (MDR)>

$$CH_4 \rightarrow C + 2H_2 + 74\ kJ/mol \quad (5)$$

<Boudouard reaction (BD)>

$$2CO \rightarrow C + CO_2 - 172\ kJ/mol \quad (6)$$

2. Numerical Simulation Procedure of BDR Membrane Reactor Using Pd/Cu Membrane and Ni/Cr Catalyst

2.1. A Mathematical Formation

COMSOL Multiphysics ver. 6.2, which is a commercial multiphysics software, allows users to customize many partial differential formulas and combine them to realize direct coupled multiphysics field analysis very easily [23]. COMSOL Muitiphysics involves the following governing formulas.

The formulas for mass conservation in porous material can be described as follows:

$$\vec{u} = -\frac{\kappa}{\mu}(\nabla p + \rho g \nabla D) \tag{7}$$

$$\nabla \cdot \left(\rho \vec{u}\right) = Q_m \tag{8}$$

$$\nabla \cdot \rho\left[-\frac{\kappa}{\mu}(\nabla p)\right] = Q_m \tag{9}$$

where $\vec{u}$ is the velocity vector [m/s], κ is the permeability [m^2], μ indicates the viscosity [Pa·s], ρ indicates the density [kg/m^3], g is the gravitational acceleration [m^2/s], D is the height [m], and Q_m is the mass source term [$kg/(m^3 \cdot s)$].

The formula for momentum conservation in porous material can be defined by the Brinkmann equation, as follows:

$$\begin{aligned} &\tfrac{\rho}{\varepsilon_p}\left(\vec{u} \cdot \nabla\right)\tfrac{\vec{u}}{\varepsilon_p} = \\ &-\nabla p + \nabla \cdot \left[\tfrac{1}{\varepsilon_p}\left\{\mu\left(\nabla \vec{u} + \left(\nabla \vec{u}\right)^T\right) - \tfrac{2}{3}\mu\left(\nabla \cdot \vec{u}\right)\vec{I}\right\}\right] - \left(\kappa^{-1}\mu + \tfrac{Q_m}{\varepsilon_p^2}\right)\vec{u} + \vec{F} \end{aligned} \tag{10}$$

where ε_p indicates the porosity [-], $\vec{I}$ indicates the unit vector [-], and $\vec{F}$ is the force vector [$kg/(m^3 \cdot s)$].

The formula of mass transfer in porous material can be defined by the Maxell–Stefan equation, as follows:

$$\nabla \cdot \left(\rho \omega_i \vec{u} - \rho \omega_i \sum_{k=1}^{n} \varepsilon_p^{\frac{3}{2}} \widetilde{D}_{ik}\left(\nabla x_k + (x_k - \omega_k)\frac{\nabla p}{p}\right) - \varepsilon_p^{\frac{3}{2}} D_i^T \frac{\nabla T}{T}\right) = R_{i,tot} \tag{11}$$

where ω_i and ω_k are the mass ratios of chemicals i and k, respectively [-], $\widetilde{D}_{ik}$ indicates Fick's diffusion coefficient of effective multicomponents [m^2/s], D_i^T indicates the thermal diffusion coefficient [$kg/(m \cdot s)$], and $R_{i,tot}$ indicates the reaction rate of chemical species [$mol/(m^3 \cdot s)$].

The formulas of heat transfer in porous material can be defined as follows:

$$\rho_f C_{p,f} \vec{u} \cdot \nabla T + \nabla \cdot \vec{q} = Q + Q_p + Q_{vd} \tag{12}$$

$$\vec{q} = -k_{eff} \nabla T \tag{13}$$

where f indicates the physical quantity of the fluid [-], C_p indicates the constant-pressure specific heat [$J/(kg \cdot K)$], $\vec{q}$ indicates the thermal flux vector [W/m^2], Q indicates the thermal source [W/m^3], Q_p indicates the thermal source caused by pressure loss [W/m^3], Q_{vd} indicates the thermal source due to viscosity dissipation [W/m^3], and k_{eff} indicates the effective thermal conductivity [$W/(m \cdot K)$].

Since there are a lot of previous studies conducted by means of COMSOL Multiphysics for numerical simulation on BDR and they report the reaction characteristics and heat and mass transfer [21–23], this study has selected COMSOL Multiphysics for the numerical simulation.

2.2. 2D Numerical Simulation Model of BDR Membrane Reactor

Figure 1 shows the schematic drawing of the 2D model. The dimensions of the reaction chamber and sweep chamber are 40 mm × 100 mm. The inlet and the outlet of the reaction chamber and sweep chamber are set in a 2D model. The length of the inlet and outlet of the reaction chamber and sweep chamber is 6 mm in Figure 1. Regarding the sweep gas flowing into the sweep chamber, Ar is adopted in this study. This study selected Ar as the sweep gas because it is an inactive gas. Ar is a popular gas to adopt as a sweep gas in the previous studies on biogas dry reforming membrane reactor [19,24–26]. Additionally, the previous experimental studies conducted by the authors [7,27] selected Ar as the sweep gas. The reason why Ar was selected as the sweep gas is because it is easy to detect air leaks when using Ar in experimental studies [7,27]. To fit the numerical simulation condition with that in the experimental studies conducted by the authors [7,27], we have set Ar as the sweep gas. The Pd/Cu membrane used for H_2 separation is located between the reaction chamber and the sweep chamber. The thicknesses of the Pd/Cu membrane were varied at 20 μm, 40 μm, and 60 μm, which was the same as the authors' previous experimental works [28,29]. This study carried out a stationary numerical simulation.

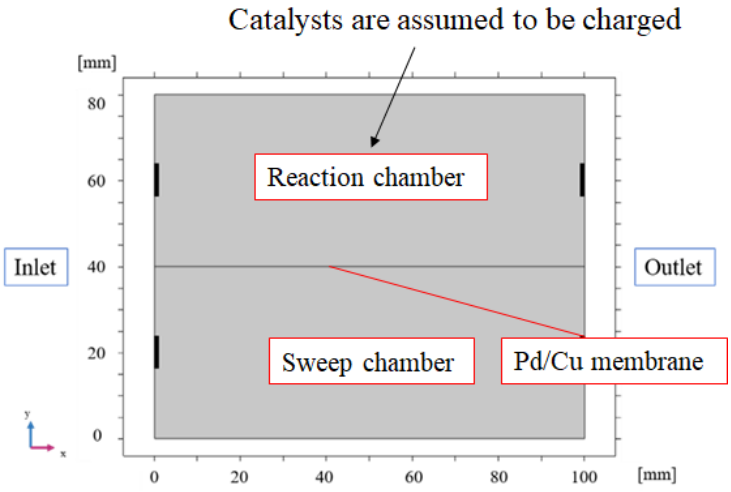


Figure 1. Schematic figure of the 2D model used for the numerical simulation in the present study.

2.3. Kinetic Model of BDR

We considered the reaction scheme exhibited by Equations (1)–(6) to conduct the numerical simulation. Reaction rates of these formulas can be defined as follows [30–32]:

<Dry reforming reaction (DR)>

$$r_1 = k_1 \cdot \left[\frac{K_{CO_2,1} K_{CH_4,1} P_{CO_2} P_{CH_4}}{\left(1 + K_{CO_2,1} P_{CO_2} + K_{CH_4,1} P_{CH4}\right)^2} \right] \cdot \left[1 - \frac{\left(P_{CO} P_{H_2}\right)^2}{K_1 P_{CO_2} P_{CH_4}} \right] \quad (14)$$

where $k_1 = 1290 \times 5000 e^{\frac{-102065}{RT}}$, $K_{CO_2,1} = 2.64 \times 10^{-2} e^{\frac{37641}{RT}}$, $K_{CH_4,1} = 2.63 \times 10^{-2} e^{\frac{40684}{RT}}$, $K_1 = e^{34.011} \cdot e^{\frac{-258598}{RT}}$.

<Reverse water gas shift reaction (RWGS)>

$$r_2 = k_2 P_{CO_2}\left(1 - \frac{P_{CO}P_{H_2O}}{K_2 P_{CO_2}P_{H_2}}\right) \tag{15}$$

where $k_2 = 9.28 \times 10^3 e^{\frac{-73105}{RT}}$, $K_2 = 68.78e^{\frac{-37500}{RT}}$.

<Steam reforming reaction (SR)>

$$r_3 = \frac{\frac{k_3}{P_{H_2}^{2.5}}\left(P_{CH_4}P_{H_2O} - \frac{P_{CO}P_{H_2}^3}{K_3}\right)}{\left(1 + \frac{P_{H_2O}K_{H_2O,2}}{P_{H_2}} + K_{CO,2}P_{CO} + K_{H_2,2}P_{H_2} + K_{CH_4,2}P_{CH_4}\right)^2} \tag{16}$$

where $k_2 = 2.636 \times 10^{12} e^{\frac{-240100}{RT}}$, $K_2 = 1.198 \times 10^{17} e^{\frac{-26830}{RT}}$, $K_{CO_2,2} = 8.23 \times 10^{-5} e^{\frac{70650}{RT}}$, $K_{CH_4,2} = 6.65 \times 10^4 e^{\frac{38280}{RT}}$, $K_{H_2,2} = 6.12 \times 10^{-9} e^{\frac{82900}{RT}}$, $K_{H_2O,2} = 1.77 \times 10^5 e^{\frac{-88680}{RT}}$.

<Methanation reaction (MR)>

$$r_4 = \frac{\frac{k_4}{P_{H_2}^{3.5}}\left(P_{CH_4}P_{H_2O}^2 - \frac{P_{CO_2}P_{H_2}^4}{K_4}\right)}{\left(1 + \frac{P_{H_2O}K_{H_2O,4}}{P_{H_2}} + K_{CO,4}P_{CO} + K_{H_2,4}P_{H_2} + K_{CH_4,4}P_{CH_4}\right)^2} \tag{17}$$

where $k_4 = 6.364 \times 10^{11} e^{\frac{-24390}{RT}}$, $K_4 = 2.117 \times 10^{15} e^{\frac{-22430}{RT}}$, $K_{CH_4,4} = 6.65 \times 10^{-4} e^{\frac{38280}{RT}}$, $K_{CO,4} = 8.23 \times 10^{-5} e^{\frac{70650}{RT}}$, $K_{H_2,4} = 6.12 \times 10^{-9} e^{\frac{82900}{RT}}$, $K_{H_2O,4} = 1.77 \times 10^5 e^{\frac{-88680}{RT}}$.

<Methane decomposition reaction (MDR)>

$$r_5 = \frac{k_5 K_{CH_4,5}\left(P_{CH_4} - \frac{P_{H_2}^2}{K_5}\right)}{\left(1 + K_{CH_4,5}P_{CH_4} + \frac{P_{H_2}^{1.5}}{K_{H_2,5}}\right)^2} \tag{18}$$

where $k_5 = 6.95 \times 10^3 e^{\frac{-58983}{RT}}$, $K_5 = 2.95 \times 10^5 e^{\frac{-84440}{RT}}$, $K_{CH_4,5} = 0.21e^{\frac{-567}{RT}}$, $K_{H_2,5} = 5.18 \times 10^7 e^{\frac{-133210}{RT}}$.

<Boudouard reaction (BD)>

$$r_6 = \frac{\frac{k_6}{K_{CO,6}K_{CO_2,6}}\left(\frac{P_{CO}}{K_6} - \frac{P_{CO_2}}{P_{CO}}\right)}{\left(1 + K_{CO,6}P_{CO} + \frac{1}{K_{CO,6}K_{CO_2,6}}\frac{P_{CO_2}}{P_{CO}}\right)^2} \tag{19}$$

where $k_6 = 1.34 \times 10^{15} e^{\frac{-243835}{RT}}$, $K_6 = 1.9393 \times 10^9 e^{\frac{-168527}{RT}}$, $K_{CO_2,6} = 2.81 \times 10^7 e^{\frac{-104085}{RT}}$, $K_{CO,6} = 7.34 \times 10^{-6} e^{\frac{100395}{RT}}$. Additionally, r_n indicates the kinetic rate (where n = 1, 2, 3, 4, 5, 6) [mol/(kg·s)], k_n indicates the kinetic constant (where n = 1, 2, 3, 4, 5, 6) [mol/(kg·s)], P_i indicates the particle pressure of chemical species i [Pa], K_n indicates the equilibrium constant (where n = 1, 2, 3, 4, 5, 6) [-], and K_i indicates the absorption equilibrium constants of chemical species i [-].

2.4. Parameters and Conditions of Numerical Simulation

The molar ratio of CH_4:CO_2 was set at 1.5:1 in this study, simulating a biogas. The initial reaction temperatures were varied at 400 °C, 500 °C, and 600 °C. This study assumed that Ni/Cr alloy metal was the catalyst adopted for the previous experimental works [7,27]. The weight ratio of Cr to the whole weight of Ni/Cr alloy metal was 20 wt.%. This study calculated the porosity, permeability, constant-pressure specific heat, and thermal conductivity of Ni/Cr alloy catalysts according to the weight ratio of Cr. The porosity (ε_p) was set at 0.95. The thicknesses of the Pd/Cu membrane were varied at 20 μm, 40 μm, and

60 μm. Table 1 shows the physical properties and parameters adopted for the numerical simulation in the present study.

Table 1. Numerical simulation conditions adopted in the present study.

Initial Reaction Temperature [°C]	400, 500, 600
Pressure of gas in reactor [Pa]	1.013×10^5
Flow rate of CH_4 at inlet [kg/s] (CH_4:CO_2 = 1.5:1)	5.78×10^{-11}
Flow rate of CO_2 at inlet [kg/s] (CH_4:CO_2 = 1.5:1)	1.23×10^{-11}
Pressure at the outlet of reactor [Pa]	1.013×10^5
Density of Ni/Cr catalyst [kg/m^3]	1045, 1042, 1040 (@400 °C, 500 °C, 600 °C)
Porosity of Ni/Cr catalyst (ε_p) [-]	0.95
Permeability of Ni/Cr catalyst [m^2]	1.7×10^{-8}, 1.6×10^{-8}, 1.5×10^{-9}
Specific heat at constant pressure of Ni/Cr catalyst [J/(kg·K)]	327, 333, 340
Thermal conductivity of Ni/Cr catalyst [W/(m·K)]	197, 194, 192

The following assumptions were set in this study:

(i) The catalyst was assumed to be a porous material. The porosity, permeability, constant-pressure specific heat, thermal conductivity, and isotropy were set to be constant.
(ii) The wall temperature was set to be isothermal.
(iii) The gas was set to be a Newton fluid and treated to be an ideal gas.
(iv) The wall of the reactor, except for the inlet and outlet, was set to be no-slip.
(v) The pressure of the outlet was set to be atmospheric pressure (gauge pressure: 0 Pa).
(vi) The temperature of the inflow gas was the same as the initial reaction temperature.
(vii) The produced carbon was assumed to be a gas.

As for (vii), solid carbon is generated according to Equations (5) and (6) generally. However, COMSOL Multiphysics utilized by the present study cannot treat a solid carbon and a gaseous carbon. Consequently, we considered assumption (vii).

2.5. Evaluation Factor for Reaction Characteristics in the Present Study

The evaluation factors defined in this study are as follows:

$$\mathrm{CH_4\ conversion} = \frac{C_{CH4,in} - C_{CH4,out}}{C_{CH4,in}} \times 100\ [\%] \tag{20}$$

where $C_{CH4,in}$ indicates the molar concentration of CH_4 at the inlet [mol] and $C_{CH4,out}$ indicates the molar concentration of CH_4 at the outlet [mol].

$$\mathrm{CO_2\ conversion} = \frac{C_{CO2,in} - C_{CO2,out}}{C_{CO2,in}} \times 100\ [\%] \tag{21}$$

where $C_{CO2,in}$ indicates the molar concentration of CO_2 at the inlet [mol] and $C_{CO2,out}$ indicates the molar concentration of CO_2 at the outlet [mol].

$$\mathrm{H_2\ yield} = \frac{\frac{1}{2}C_{H2,out}}{C_{CH4,in}} \times 100\ [\%] \tag{22}$$

where $C_{H2,out}$ indicates the molar concentration of H_2 at the outlet [mol].

$$\mathrm{H_2\ selectivity} = \frac{C_{H2,out}}{C_{H2,out} + C_{CO,out}} \times 100\ [\%] \tag{23}$$

where $C_{CO,out}$ indicates the molar concentration of CO at the outlet [mol].

$$\text{CO selectivity} = \frac{C_{CO,out}}{C_{H2,out} + C_{CO,out}} \times 100\ [\%] \quad (24)$$

3. Results and Discussion

3.1. Comparison of the Distriburtion of Pressure Along X-Direction Among Different Initial Reaction Temperatures and Thicknesses of Pd/Cu Membranes

Figure 2 shows the comparison of the distribution of pressure along the *x*-direction in the reaction chamber (y = 62 mm), Pd/Cu membrane (y = 40 mm), and sweep chamber (y = 20 mm) with the change in the initial reaction temperature. In this figure, the thickness of the Pd/Cu membrane is 20 μm.

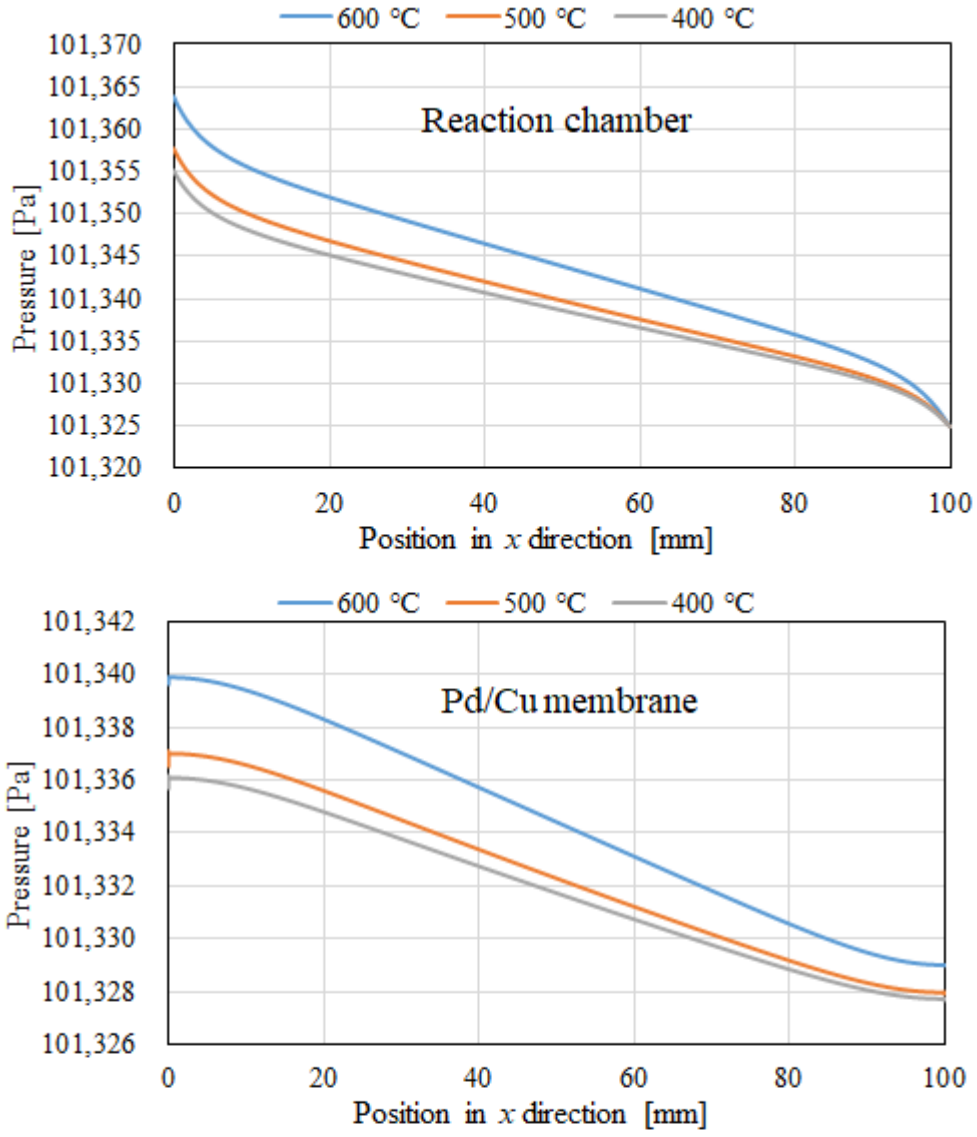


Figure 2. *Cont.*

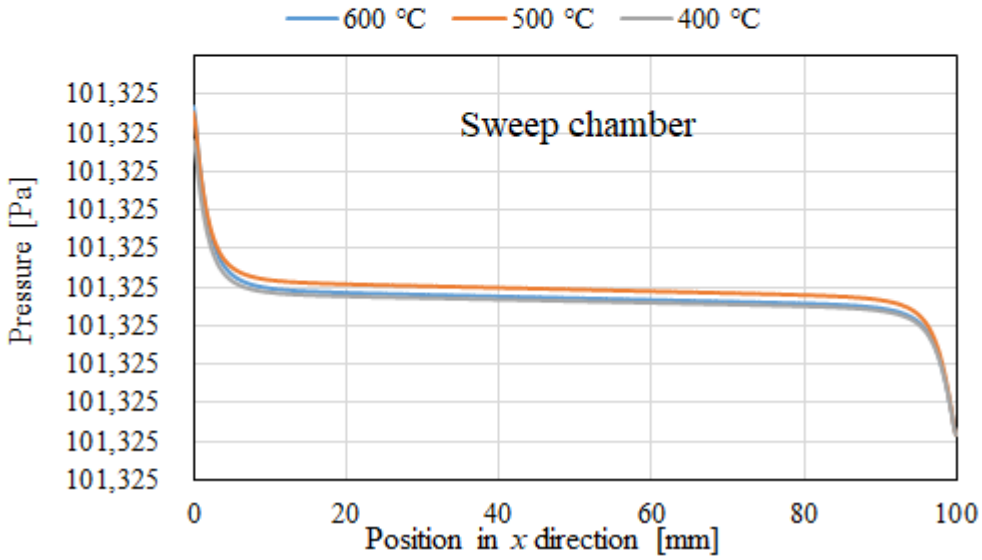


Figure 2. Impact of the initial reaction temperature on the distribution of pressure along the *x*-direction in the reaction chamber (y = 62 mm), Pd/Cu membrane (y = 40 mm), and sweep chamber (y = 20 mm).

It is seen from Figure 2 that the pressure in the reaction chamber as well as the Pd/Cu membrane decreases along the *x*-direction. This is due to the permeation resistance of the porous catalyst and Pd/Cu membrane. Additionally, we can know that the pressure in the reaction chamber and Pd/Cu membrane rises with the rise in the initial reaction temperature. It is thought from the state equation, i.e., $pV = nRT$, that pressure rises with the increase in the temperature. Moreover, the difference in the initial pressure (at x = 0 mm) among the different initial temperatures is provided by the rise in pressure because of the volume change caused by the change in the initial reaction temperature. It can be thought from the state equation, i.e., $pV = nRT$, that the pressure increases with the rise in temperature. Moreover, the pressures near the inlet and the outlet changes rapidly, especially for those in the sweep chamber. Since the length of the inlet and outlet of the reaction chamber and sweep chamber is 6 mm, which is shorter than the height of the reaction chamber and sweep chamber of 40 mm, the large pressure change occurs due to the change in cross-sectional area for the gas flow.

Figure 3 shows the comparison of the distribution of pressure along the *x*-direction in the reaction chamber (y = 62 mm), Pd/Cu membrane (y = 40 mm), and sweep chamber (y = 20 mm) with varying thickness of the Pd/Cu membrane. In Figure 3, the results obtained at the initial reaction temperature of 600 °C are shown. It is seen from Figure 3 that the pressure in the reaction chamber and Pd/Cu membrane decreases along the *x*-direction. This is due to the permeation resistance of the porous catalyst and Pd/Cu membrane. According to Figure 3, the pressure in the Pd/Cu membrane is higher with the decrease in the thickness of the Pd/Cu membrane, though the influence of the thickness of the Pd/Cu membrane on the pressure in the reaction chamber and sweep chamber is very small. Since the permeation resistance decreases with the decrease in the thickness of the Pd/Cu membrane, the pressure in the Pd/Cu membrane is higher. In Figure 3, the initial reaction temperature was set at 600 °C, which was the same temperature as in the reaction chamber and sweep chamber. Since the initial temperature was the same in the different experiment with various thicknesses of Pd/Cu membranes, we could consider that the change in pressure in the reaction chamber and sweep chamber was small. Regarding the pressure drop across the Pd/Cu membrane, it reduced with the decrease in the thickness of the Pd/Cu membrane because of the reduction in the permeation resistance of the Pd/Cu membrane.

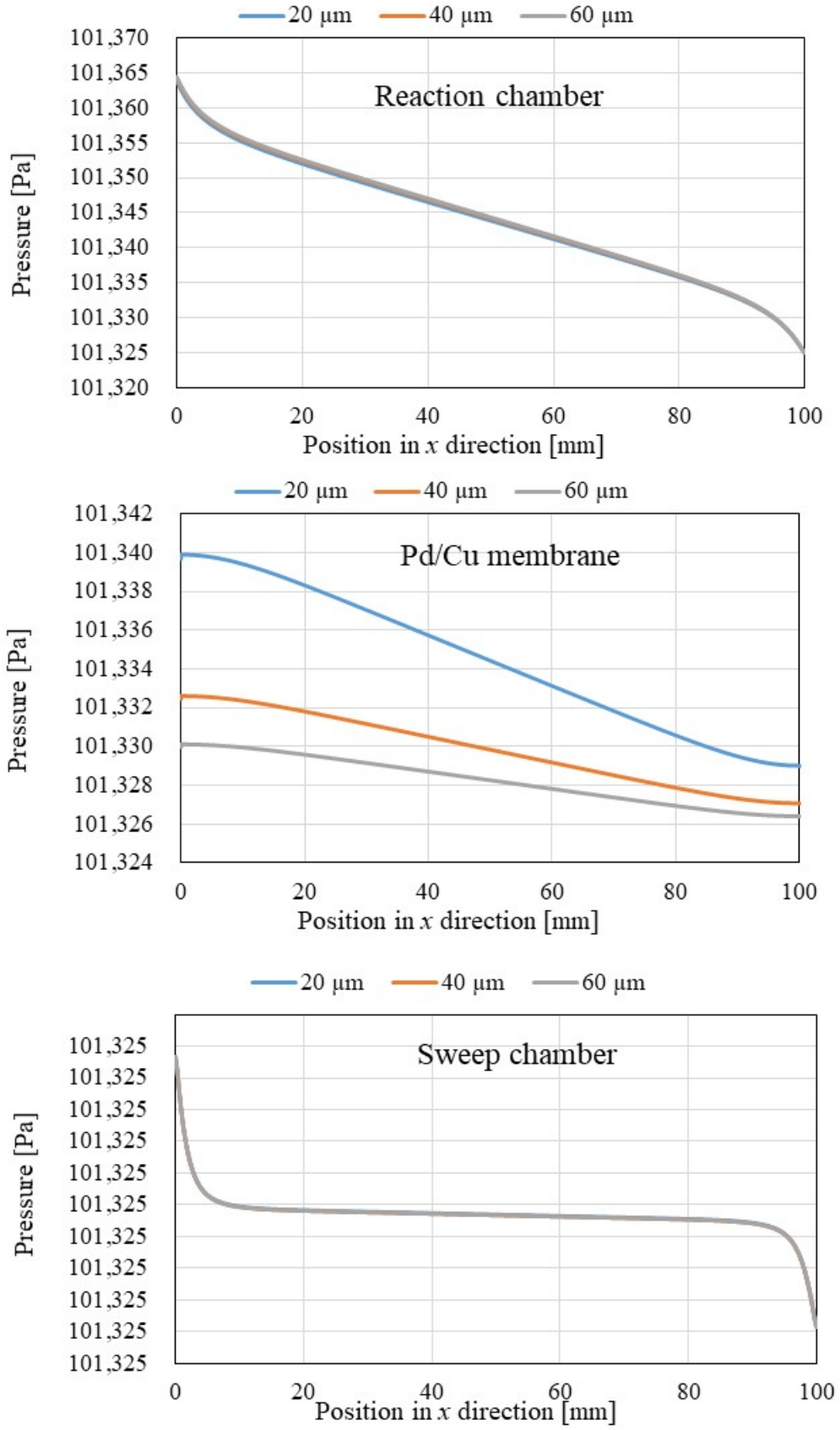


Figure 3. Influence of the thickness of the Pd/Cu membrane on the distribution of pressure along the *x*-direction in the reaction chamber (y = 62 mm), Pd/Cu membrane (y = 40 mm), and sweep chamber (y = 20 mm).

3.2. Comparison of Gas Concentrations Along X-Direction Among Different Initial Reaction Temperatures and Thicknesses of Pd/Cu Membranes

Figure 4 displays the comparison of the distribution of gas concentrations along the-direction in the reaction chamber (y = 62 mm) among different initial reaction temperatures. The thickness of the Pd/Cu membrane is 20 μm in this figure. From Figure 4, it is clear that the molar concentrations of CH_4 and CO_2 decrease with the increase in the initial reaction temperature, while the molar concentrations of H_2, CO, H_2O, and C rise with the rise in the initial reaction temperature. From the present study, the reaction rates of the considered reactions can be shown by the Arrhenius type as displayed in Equations (14)–(19). Consequently, the amounts of products, i.e., H_2, CO, H_2O, and C, increased with the rise in the initial reaction temperature. Moreover, Equation (1) is an endothermic reaction, meaning it can be thought that the molar concentrations of CH_4 and CO_2 decrease and those of H_2 and CO rise with the rise in the initial reaction temperature. Regarding the formation of H_2O and C, it is thought that Equations (3)–(6) might occur. The formation of H_2O and C were observed by the authors' previous experimental study [28]. After the experiments, carbon was observed as shown in Figure 5 [27]. On the other hand, the formation of H_2O was confirmed by means of observation using the gas bag exhibited in Figure 6. From the review paper of the authors' literature survey, there are a lot of previous studies reporting CH_4 dry reforming with a reverse H_2O gas shift [29]. These review papers reported high CH_4 and CO_2 conversions and H_2 yield, e.g., CH_4 conversion of 43.0–98.6%, CO_2 conversion of 4.0–98.5%, and H_2 yield of 2.62–94.9%, respectively [29]. Consequently, we think that the presence of H_2O is not a bad indicator for such a relatively atmospheric-based reaction.

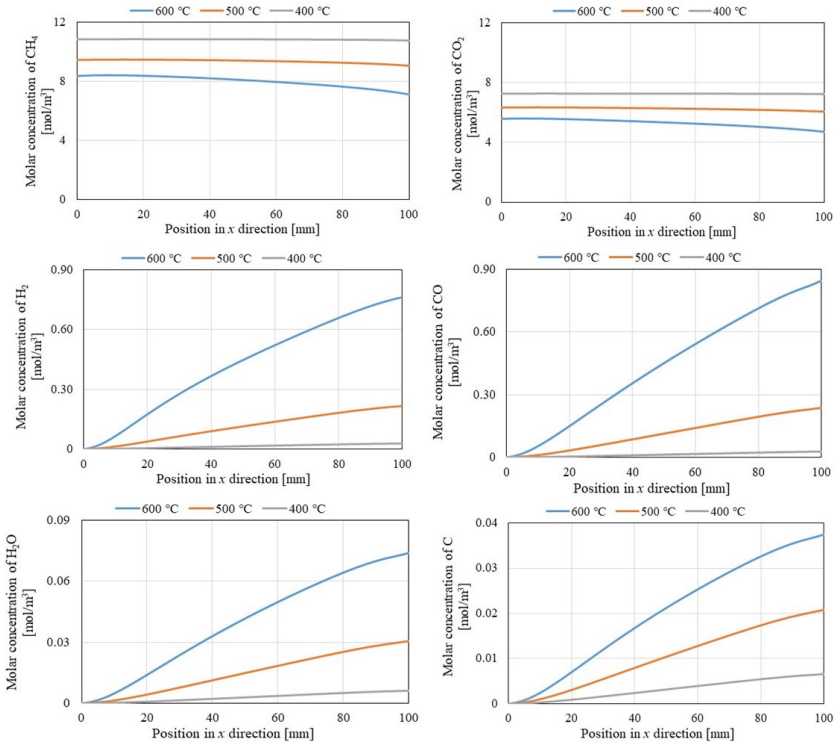


Figure 4. Impact of the initial reaction temperature on the distribution of the gas concentrations along the x-direction in the reaction chamber (y = 62 mm).

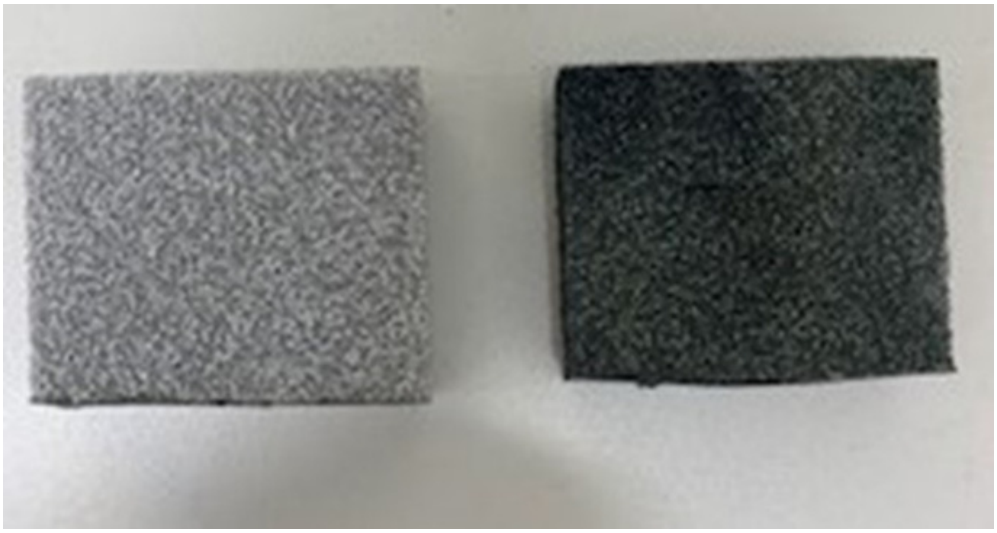


Figure 5. Photo of Ni/Cr catalyst used in this study before and after experiments (left catalyst: before experiment; right catalyst: after experiment) [27].

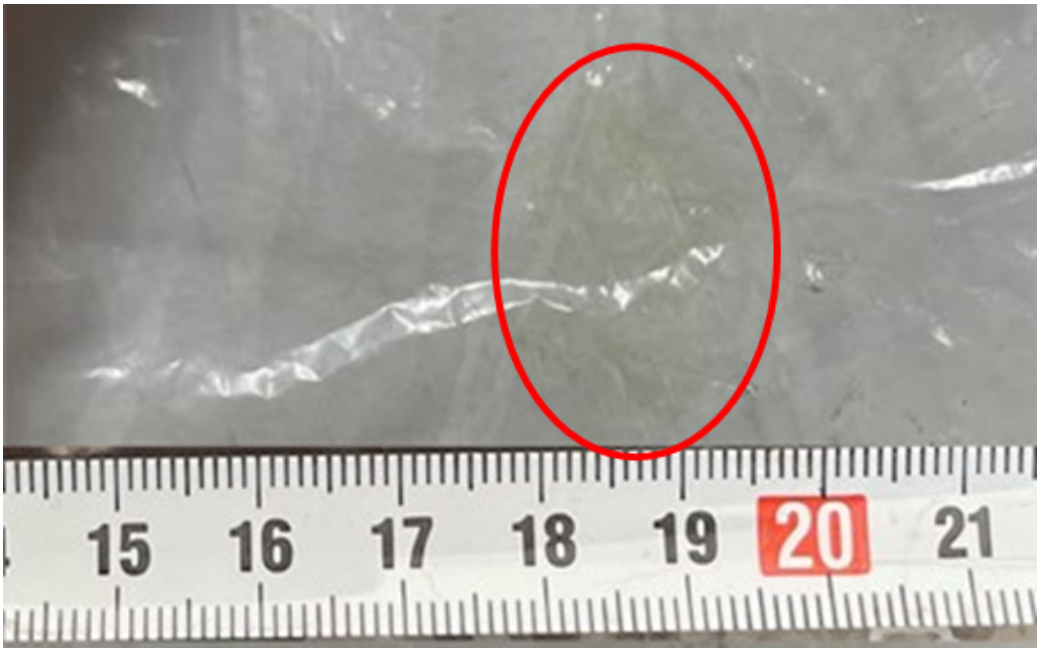


Figure 6. Photo of produced H_2O observed using gas bag [27].

Figure 7 shows the influence of the initial reaction temperature on the distributions of the molar concentration of H_2 along the x-direction in the reaction chamber (y = 62 mm), Pd/Cu membrane (y = 40 mm), and sweep chamber (y = 20 mm). It is seen from Figure 7 that the molar concentration of H_2 rises along the x-direction in the reaction chamber, Pd/Cu membrane, and sweep chamber. Since the H_2 production reactions, i.e., Equations (1), (2) and (5), occur along the x-direction, the molar concentration of H_2 rises along the x-direction. Moreover, it is observed that the molar concentration of H_2 in the reaction chamber, Pd/Cu membrane, and sweep chamber rises with the rise in the initial reaction temperature. Because the H_2 production reactions, i.e., Equations (1), (2) and (5), are endothermic reactions, the molar concentration of H_2 increases with the rise in the initial reaction temperature. Additionally, it is known from Figure 7 that the molar concentrations of H_2 in the Pd/Cu membrane and sweep chamber are higher when the molar concentration of H_2 in the reaction chamber is higher. The molar concentration of H_2 in the reaction chamber is higher, resulting in the driving force to permeate the Pd/Cu membrane becoming

stronger because of the high H_2 partial pressure difference between the reaction chamber and the sweep chamber [28]. The molar concentrations of H_2 in the Pd/Cu membrane and sweep chamber are higher.

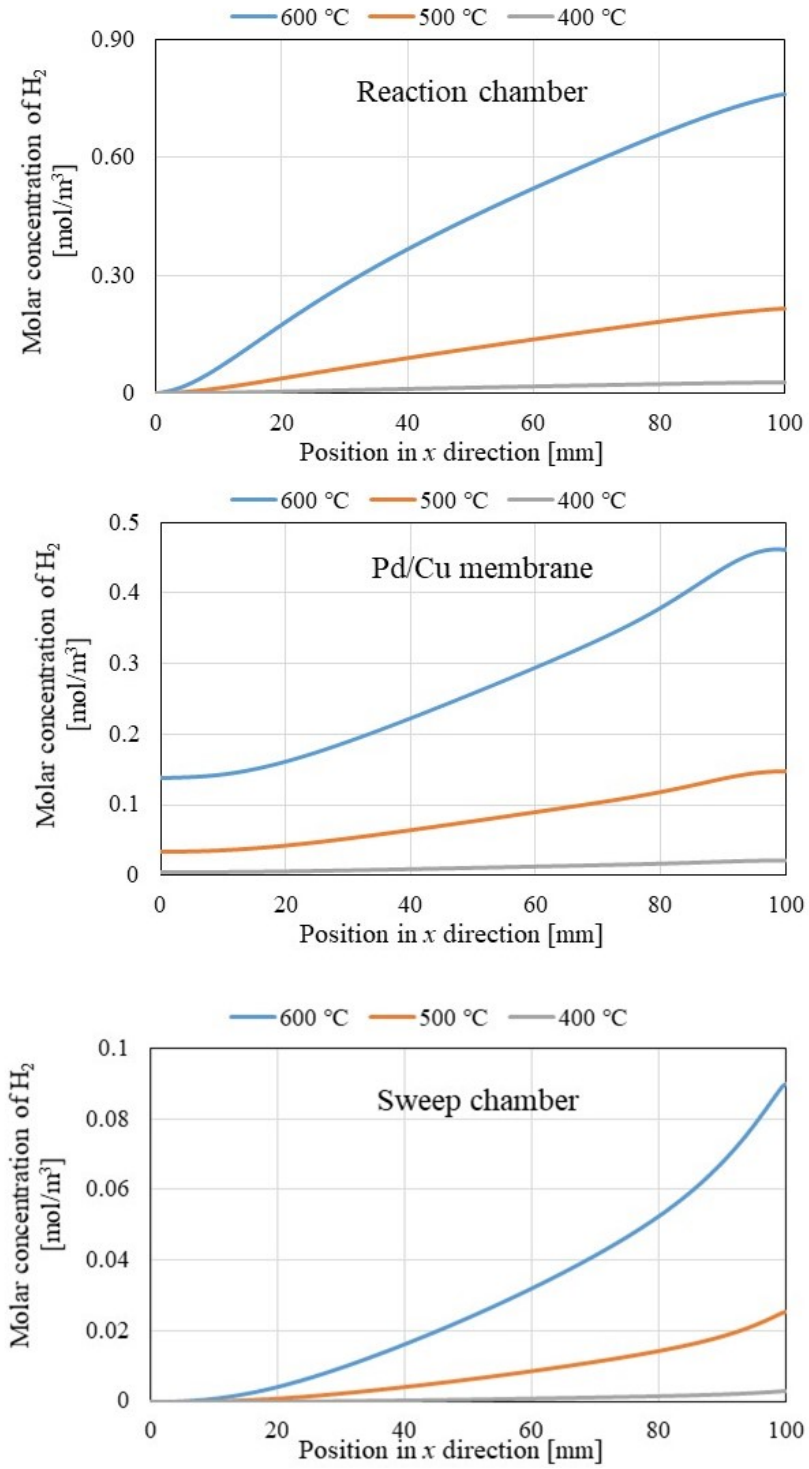


Figure 7. Influence of the initial reaction temperature on the distribution of molar concentrations of H_2 along the x-direction in the reaction chamber (y = 60 mm), Pd/Cu membrane (y = 40 mm), and sweep chamber (y = 20 mm).

Figure 8 shows the comparison of the distributions of each gas concentration along the x-direction in the reaction chamber (y = 62 mm) among different thicknesses of Pd/Cu membranes. It is seen from Figure 8 that the influence of the thickness of the Pd/Cu

membrane on gas concentrations along the-direction in the reaction chamber is small. However, it can be revealed that the molar concentrations of H_2 in the Pd/Cu membrane and sweep chamber rise with the decrease in the thickness of the Pd/Cu membrane according to Figure 9. The penetration resistance of the Pd/Cu membrane decreases with the decrease in the thickness of the Pd/Cu membrane, resulting in the molar concentrations of H_2 in the Pd/Cu membrane and sweep increasing with the decrease in the thickness of the Pd/Cu membrane.

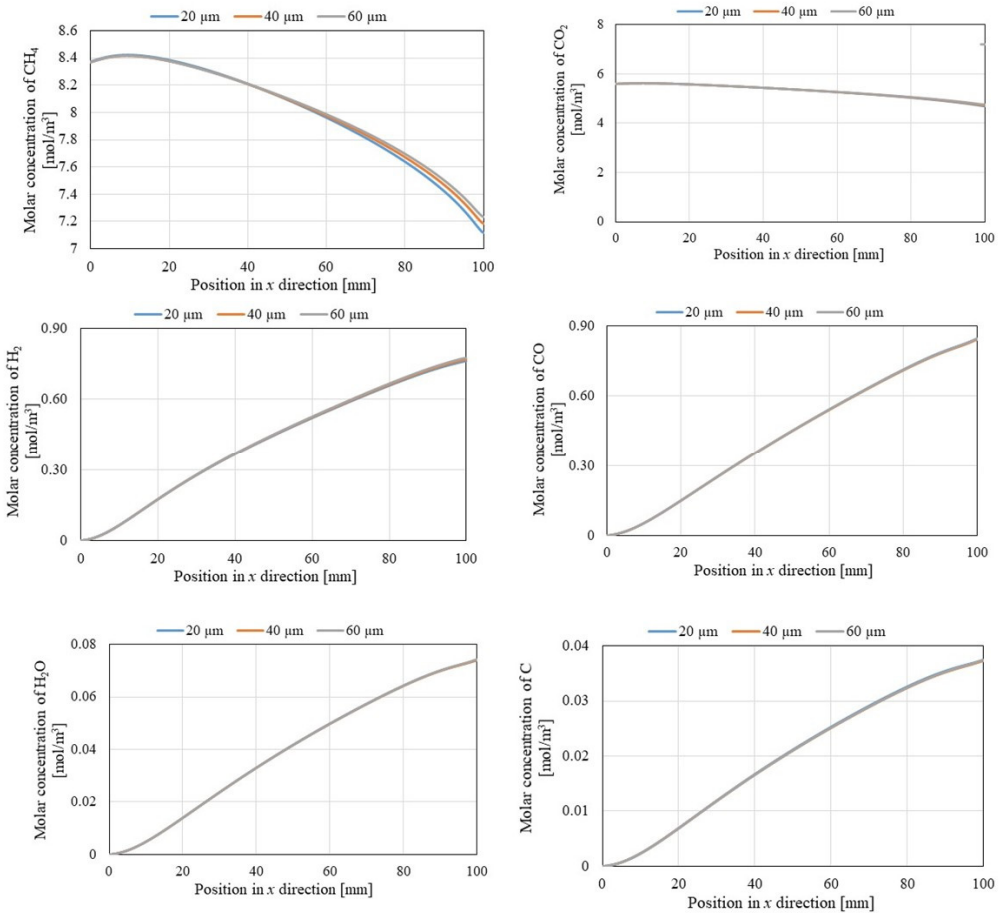


Figure 8. Influence of the thickness of the Pd/Cu membrane on the distribution of gas concentrations along the *x*-direction in the reaction chamber (y = 62 mm).

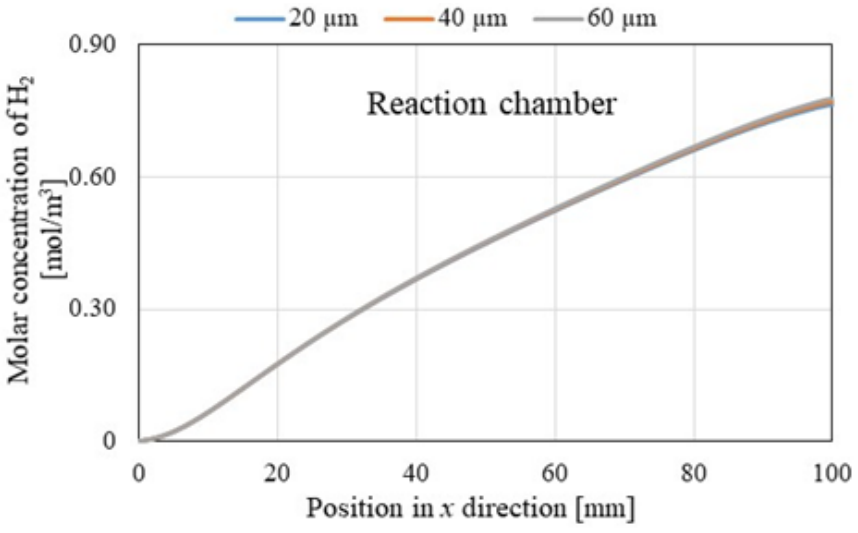


Figure 9. *Cont*.

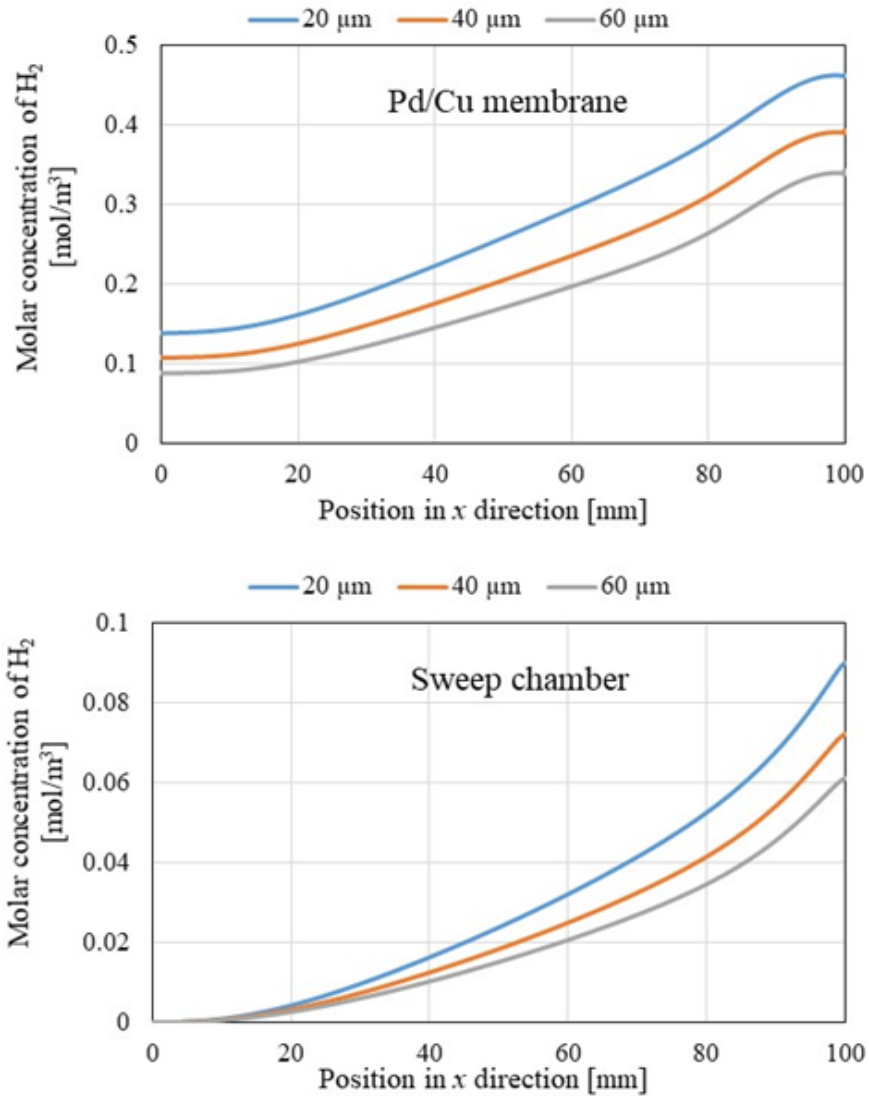


Figure 9. Influence of the thickness of the Pd/Cu membrane on the distribution of the molar concentration of H_2 along the *x*-direction in the reaction chamber (*y* = 60 mm), Pd/Cu membrane (*y* = 40 mm), and sweep chamber (*y* = 20 mm).

3.3. Investigation on Reaction Characteristics by Evaluation Factors

To investigate the reaction characteristics of BDR with the other reactions considered in this study, Table 2 lists CH_4 conversion, CO_2 conversion, H_2 yield, H_2 selectivity, and CO selectivity for various initial temperatures using the thickness of the Pd/Cu membrane of 20 μm and various thicknesses of Pd/Cu membranes at the initial temperature of 600 °C.

Table 2. Comparison of CH_4 conversion, CO_2 conversion, H_2 yield, H_2 selectivity, and CO selectivity for various initial temperatures using the thickness of the Pd/Cu membrane of 20 μm and various thicknesses of Pd/Cu membranes at the initial temperature of 600 °C.

Thickness of Pd/Cu membrane of 20 μm					
Initial Reaction Temperature [°C]	CH_4 Conversion [%]	CO_2 Conversion [%]	H_2 Yield [%]	H_2 Selectivity [%]	CO Selectivity [%]
600	15.0	15.9	5.09	49.1	50.9
500	4.03	3.73	1.14	46.4	53.6
400	1.10	0.49	0.15	52.2	47.8
Initial Temperature of 600 °C					
Thickness of Pd/Cu Membrane [μm]	CH_4 Conversion [%]	CO_2 Conversion [%]	H_2 Yield [%]	H_2 Selectivity [%]	CO Selectivity [%]
20	15.0	15.9	5.09	49.1	50.9
40	14.2	15.4	5.02	49.2	50.8
60	13.5	15.0	5.00	49.2	50.8

According to Table 2, it can be clear that CH_4 conversion, CO_2 conversion, and H_2 yield increase with the increase in the initial reaction temperature. Because Equations (1)–(3) and (5) are endothermic reactions, the consumption of CH_4, CO_2, and the production of H_2 increase more with the increase in the initial reaction temperature. Additionally, it is clear from Table 2 that CH_4 conversion, CO_2 conversion, and H_2 yield rise with the decrease in the thickness of the Pd/Cu membrane. The penetration resistance of the Pd/Cu membrane decreases with the decrease in the thickness of the Pd/Cu membrane, resulting in the permeation of H_2 through the Pd/Cu membrane being promoted. Then, it is thought that Equations (1), (2) and (5), which are reactions producing H_2, are in a non-equilibrium state. Therefore, the consumption of CH_4 and CO_2 and the production of H_2 rise more with the decrease in the thickness of the Pd/Cu membrane. According to Equation (5), C is produced more if the reaction is in a non-equilibrium state by separating H_2 from the reaction chamber via the Pd/Cu membrane. This phenomenon is confirmed by Figure 4.

According to the literature review, there was no H_2 embrittment in the Pd/Cu membrane observed [32,33]. The Pd/Cu membrane exhibited a constant H_2/N_2 selectivity in the excess of 7000 over 70 days [33]. In addition, the change in the performance and shape of the Pd/Cu membrane was not observed after the experiments over 250 h [25]. Therefore, H_2 embrittment of the Pd/Cu membrane was not thought to be the reason why less H_2 was produced using the Pd/Cu membrane in the present study.

As explained in introduction, the previous studies reported that CH_4 conversion and CO_2 conversion are approximately 40–100% and 50–100%, respectively [8–15]. These values of CH_4 conversion and CO_2 conversion are higher than those obtained in this study. This study thinks that the initial reaction temperature of 600 °C is not sufficient to achieve a better performance of BDR, which is compared to previous studies [8–15]. From the previous reports with Ni alloy catalysts, CH_4 conversion, H_2 yield, and H_2 selectivity rose with the rise in the initial reaction temperature, and larger values were observed over 600 °C [9,23,31,34]. This study proposes that the following subjects can be considered to enhance the performance of H_2 production: (i) optimizing the catalyst shape and composition, (ii) optimizing the thickness and composition of the Pd/Cu membrane, and (iii) optimizing the H_2 separation rate of the Pd/Cu membrane and the H_2 production rate of the catalyst. This study would like to investigate these subjects.

4. Conclusions

We have clarified the performance of a BDR membrane reactor using a Pd/Cu membrane and an Ni/Cr catalyst by means of the COMSOL Multiphysics numerical simulation. The initial reaction temperatures studied were varied at 400 °C, 500 °C, and 600 °C. The thicknesses of the Pd/Cu membrane in the study were varied at 20 μm, 40 μm, and 60 μm. As a result, the following findings were obtained:

(i) The pressure in the reaction chamber and Pd/Cu membrane decreased along the *x*-direction and they rose with the increase in the initial reaction temperature.
(ii) The pressure in the Pd/Cu membrane rose with the decrease in the thickness of the Pd/Cu membrane, though the influence was very small.
(iii) It can be revealed that the molar concentrations of CH_4 and CO_2 decreased with the rise in the initial reaction temperature, while the molar concentrations of H_2, CO, H_2O, and C increased with the increase in the initial reaction temperature. Moreover, the formed H_2O and C demonstrate that Equations (3)–(6) occurred.
(iv) The molar concentration of H_2 rose along the *x*-direction of the reaction chamber, Pd/Cu membrane, and sweep chamber. Since the H_2 production reactions, i.e., Equations (1), (2) and (5), occur along the *x*-direction, the molar concentration of H_2 increasing along the *x*-direction was expected.
(v) The molar concentrations of H_2 in the reaction chamber, Pd/Cu membrane, and sweep chamber increased with the increase in the initial reaction temperature.
(vi) The molar concentrations of H_2 in the Pd/Cu membrane and sweep chamber were higher when the molar concentration of H_2 in the reaction chamber was higher.
(vii) It is clear that the molar concentrations of H_2 in the Pd/Cu membrane and sweep chamber rose with the decrease in the thickness of the Pd/Cu membrane.
(viii) The CH_4 conversion, CO_2 conversion, and H_2 yield rose with the increase in the initial reaction temperature and the reduction in the thickness of the Pd/Cu membrane.

Author Contributions: Conceptualization and writing—original draft preparation, A.N.; methodology and software, R.I. and S.Y.; data curation, M.I. and T.H.; writing—review and editing, E.H. All authors have read and agreed to the published version of the manuscript.

Funding: This study was funded by KRI cooperation.

Data Availability Statement: The authors agree to share the data of the paper published in this journal.

Conflicts of Interest: The authors do declare no conflicts of interest.

References

1. Pei, A.; Xie, R.; Zhang, Y.; Feng, Y.; Wang, W.; Zhang, S.; Huang, Z.; Zhu, L.; Chai, G.; Yang, Z.; et al. Effective electronic tuning of Pt single atoms via heterogeneous atomic coordination of (Co, Ni)$(OH)_2$ for efficient hydrogen evolution. *Energy Environ. Sci.* **2023**, *16*, 1035–1048. [CrossRef]
2. Pei, A.; Zhu, L.; Huang, Z.; Ye, J.; Chang, Y.C.; Osman, S.M.; Pao, C.W.; Gao, Q.; Chen, B.H.; Luque, R. Nickel hydroxide-supported Ru single atoms and Pd nanoclusters for enhanced electrocatalytic hydrogen evolution and ethanol oxidation. *Adv. Funct. Mater.* **2022**, *32*, 2208587. [CrossRef]
3. Wu, F.; Zeng, L.; Pei, A.; Feng, Y.; Zhu, L. N, P co-doped graphene-supported monometallic nanoparticles for highly efficient hydrogen evolution by acid electrolysis of water. *J. Mater. Chem. A* **2024**, *17*, 10300–10306. [CrossRef]
4. Kalai, D.Y.; Stangeland, K.; Jin, R.; Tucho, W.M.; Yu, Z. Biogas dry reforming for syngas production on La promoted hydrotalcite-derived Ni catalyst. *Int. J. Hydrogen Energy* **2018**, *43*, 19438–19450. [CrossRef]
5. World Bioenergy Association. Available online: https://worldbioenergy.org/global-bioenergy-statistics (accessed on 12 December 2024).
6. The Japan Gas Association. Available online: https://www.gas.or.jp/gas-life/biogas/ (accessed on 12 December 2024).
7. Nishimura, A.; Hayashi, Y.; Ito, S.; Kolhe, M.L. Performance analysis of hydrogen production for a solid oxide fuel cell system using a biogas dry reforming membrane reactor with Ni and Ni/Cr catalysts. *Fuels* **2023**, *4*, 295–313. [CrossRef]

8. Dogan, M.Y.; Arbag, H.; Tasdemir, M.; Yasyerli, N.; Yasyerli, S. Effect of ceria content in Ni-Ce-Al catalyst on catalytic performance and carbon/coke formation in dry reforming of CH_4. *Int. J. Hydrogen Energy* **2023**, *48*, 23013–23030. [CrossRef]
9. Kiani, P.; Meshksar, M.; Rahimpour, M.R. Biogas reforming over La-promoted Ni/SBA-16 catalyst for syngas production: Catalytic structure and process activity investigation. *Int. J. Hydrogen Energy* **2023**, *48*, 6262–6274. [CrossRef]
10. Carrasco-Ruiz, S.; Zhang, Q.; Gandara-Loe, J.; Pastor-Perez, L.; Odriozola, J.A.; Reina, T.R.; Bobadilla, L.F. H_2-rich syngas production from biogas reforming: Overcoming coking and sintering using bimetallic Ni-based catalysts. *Int. J. Hydrogen Energy* **2023**, *48*, 27907–27917. [CrossRef]
11. Ponugoti, P.V.; Pathmanathan, P.; Rapolu, J.; Gomathi, A.; Janardhanan, V.M. On the stability of Ni/γ-Al_2O_3 catalyst and the effect of H_2O and O_2 during biogas reforming. *Appl. Catal. A Gen.* **2023**, *651*, 119033. [CrossRef]
12. Martin-Espejo, J.L.; Merkouri, L.P.; Gandara-Loe, J.; Odriozola, J.A.; Reina, T.R.; Pastor-Perez, L. Nickel-based cerium zirconate inorganic complex structures for CO_2 valorisation via dry reforming of methane. *J. Environ. Sci.* **2024**, *140*, 12–23. [CrossRef]
13. Cao, A.N.T.; Nguyen, H.H.; Pham, T.P.T.; Pham, L.K.H.; Phuong, D.H.L.; Nguyen, N.A.; Vo, D.V.N.; Pham, P.T.H. Insight into the role of material basicity in the coke formation and performance of Ni/Al_2O_3 catalyst for the simulated-biogas dry reforming. *J. Energy Inst.* **2023**, *108*, 101252. [CrossRef]
14. Veiga, S.; Romero, M.; Faccio, R.; Segobia, D.; Apesteguia, C.; Perez, A.L.; Brondino, C.D.; Bussi, J. Biogas dry reforming over Ni-La-Ti catalysts for synthesis gas production: Effects of preparation method and biogas composition. *Fuel* **2023**, *346*, 128300. [CrossRef]
15. Cherbanski, R.; Kotkowski, T.; Molga, E. Thermogravimetric analysis of coking during dry reforming of methane. *Int. J. Hydrogen Energy* **2023**, *48*, 7346–7360. [CrossRef]
16. Nishimura, A.; Yamada, S.; Ichii, R.; Ichikawa, M.; Hayakawa, T.; Kolhe, M.L. Hydrogen yield enhancement in biogas dry reforming with a Ni/Cr catalyst: A numerical study. *Energies* **2024**, *17*, 5421. [CrossRef]
17. Jokar, S.M.; Farokhnia, A.; Tavakolian, M.; Pejman, M.; Parvasi, P.; Javanmardi, J.; Zare, F.; Clara Gonqalves, M.; Basile, A. The recent areas of applicability of palladium based membrane technologies for hydrogen production from methane and natural gas: A review. *Int. J. Hydrogen Energy* **2023**, *48*, 6451–6476. [CrossRef]
18. Bang, G.; Moon, D.K.; Kang, J.H.; Han, Y.J.; Kim, K.M.; Lee, C.H. High-purity hydrogen production via a water-gas-shift reaction in a palladium-copper catalytic membrane reactor integrated with pressure swing adsorption. *Chem. Eng. J.* **2021**, *411*, 128473. [CrossRef]
19. Lee, S.; Lim, H. The power of molten salt in methane dry reforming: Conceptual design with a CFD study. *Chem. Eng. Process.-Process Intersif.* **2021**, *159*, 108230. [CrossRef]
20. Lee, S.; Lim, H. The effect of changing the number of membranes in methane carbon dioxide reforming: A CFD study. *Int. J. Eng. Chem.* **2020**, *87*, 110–119. [CrossRef]
21. Ghasemazadeh, K.; Ghahremani, M.; Amiri, T.Y.; Basile, A. Performance evaluation of Pd-Ag membrane reactor in glyceol steam reforming process: Development of the CFD model. *Int. J. Hydrogen Energy* **2019**, *44*, 1000–1009. [CrossRef]
22. Lee, B.; Lee, S.; Lim, K. Numerical modeling studies for a methane dry reforming in a membrane reactor. *J. Nat. Gas. Sci. Eng.* **2016**, *34*, 1251–1261. [CrossRef]
23. Nishimura, A.; Mishima, D.; Ito, S.; Konbu, T.; Hu, E. Impact of separator thickness on relationship between temperature distribution and mass & current density distribution in single HT-PEMFC. *Therm. Sci. Eng.* **2023**, *6*, 4424. [CrossRef]
24. Bian, Z.; Xia, H.; Wang, Z.; Jian, B.; Yu, Y.; Yu, K.; Zhong, W.; Kawi, S. CFD simulation of a hydrogen-permeable membrane reactor for CO_2 reforming of CH_4: The interplay of the reaction and hydrogen permeation. *Energy Fuels* **2020**, *34*, 12366–12378. [CrossRef]
25. Anzelmo, B.; Wilcox, J.; Liguori, S. Hydrogen production via natural steam reforming in a Pd-Au membrane reactor. Comparison between methane and natural gas steam reforming reactions. *J. Membr. Sci.* **2018**, *568*, 113–120. [CrossRef]
26. Bosko, M.L.; Munera, J.F.; Lombardo, E.A.; Cornaglia, L.M. Dry reforming of methane in membrane reactors using Pd and Pd-Ag composite membranes on a NaA zeolite modified porous stainless steel support. *J. Membr. Sci.* **2010**, *364*, 17–26. [CrossRef]
27. Nishimura, A.; Ito, S.; Ichikawa, M.; Kolhe, M.L. Impact of thickness of Pd/Cu membrane on performance of biogas dry reforming membrane reactor utilizing Ni/Cr catalyst. *Fuels* **2024**, *5*, 439–457. [CrossRef]
28. Amini, A.; Sedaghat, M.H.; Jamshidi, S.; Shariati, A.; Rahimpour, M.R. A Comprehensive CFD simulation of an industrial-scale side-fired steam methane reformer to enhance hydrogen production. *Chem. Eng. Process.* **2023**, *184*, 109269. [CrossRef]
29. Bengerbaa, Y.; Virginieb, M.; Dumas, C. Computational fluid dynamics study of the dry reforming of methane over Ni/Al_2O_3 catalyst in membrane reactor—Coke deposition. *Kinet. Catal.* **2017**, *58*, 345–355. [CrossRef]
30. Roa, F.; Way, J.D. Influence of alloy composition and membrane fabrication on the pressure dependence of the hydrogen flux of palladium-copper membranes. *Ind. Eng. Chem. Res.* **2003**, *42*, 5827–5835. [CrossRef]
31. Kaviani, M.; Rezaei, M.; Alavi, S.M.; Akbari, E. Biogas dry reforming over nickel-silica sandwiched core-shell catalyst with various shell thickness. *Fuel* **2024**, *355*, 129533. [CrossRef]

32. Georgiadis, A.G.; Siakavelas, G.I.; Tsiotsias, A.I.; Charisous, N.D.; Ehrhardt, B.; Wang, W.; Sebastian, V.; Hinder, S.J.; Baker, M.A.; Mascotto, S.; et al. Biogas dry reforming over Ni/LnO_x-type catalysts (Ln = La, Ce, Sm or Pr). *Int. J. Hydrogen Energy* **2023**, *48*, 19953–19971. [CrossRef]
33. Kumar, R.; Kumar, A.; Pal, A. Overview of hydrogen production from biogas reforming: Technological advancement. *Int. J. Hydrogen Energy* **2022**, *47*, 34831–34855. [CrossRef]
34. Rosha, P.; Rosha, A.K.; Ibrahim, H.; Kumar, S. Recent advances in biogas upgrading to value added products: A review. *Int. J. Hydrogen Energy* **2021**, *46*, 21318–21337. [CrossRef]

Disclaimer/Publisher's Note: The statements, opinions and data contained in all publications are solely those of the individual author(s) and contributor(s) and not of MDPI and/or the editor(s). MDPI and/or the editor(s) disclaim responsibility for any injury to people or property resulting from any ideas, methods, instructions or products referred to in the content.